PLOS | ONE

RESEARCH ARTICLE

The Subcortical Cocktail Problem; Mixed Signals from the Subthalamic Nucleus and Substantia Nigra

Gilles de Hollander[1☯], **Max C. Keuken**[1,2☯], **Birte U. Forstmann**[1*]

1 Amsterdam Brain & Cognition Center, University of Amsterdam, Amsterdam, Netherlands, **2** Max Planck Institute for Human Cognitive and Brain Sciences, Leipzig, Germany

☯ These authors contributed equally to this work.
* buforstmann@gmail.com

Citation: de Hollander G, Keuken MC, Forstmann BU (2015) The Subcortical Cocktail Problem; Mixed Signals from the Subthalamic Nucleus and Substantia Nigra. PLoS ONE 10(3): e0120572. doi:10.1371/journal.pone.0120572

Academic Editor: Bogdan Draganski, Centre Hospitalier Universitaire Vaudois Lausanne - CHUV, UNIL, SWITZERLAND

Received: August 17, 2014

Accepted: February 3, 2015

Published: March 20, 2015

Data Availability Statement: All relevant data are uploaded to the NITRC database at http://www.nitrc.org/frs/?group_id=653&release_id=2096.

Funding: This work was supported by a VIDI (BUF) grant from the Netherlands Organization for Scientific Research (NWO) and an ERC starter grant (BUF). The funders had no role in study design, data collection and analysis, decision to publish, or preparation of the manuscript.

Competing Interests: The authors declare no competing financial interest.

Abstract

The subthalamic nucleus and the directly adjacent substantia nigra are small and important structures in the basal ganglia. Functional magnetic resonance imaging studies have shown that the subthalamic nucleus and substantia nigra are selectively involved in response inhibition, conflict processing, and adjusting global and selective response thresholds. However, imaging these nuclei is complex, because they are in such close proximity, they can vary in location, and are very small relative to the resolution of most fMRI sequences. Here, we investigated the consistency in localization of these nuclei in BOLD fMRI studies, comparing reported coordinates with probabilistic atlas maps of young human participants derived from ultra-high resolution 7T MRI scanning. We show that the fMRI signal reported in previous studies is likely not unequivocally arising from the subthalamic nucleus but represents a mixture of subthalamic nucleus, substantia nigra, and surrounding tissue. Using a simulation study, we also tested to what extent spatial smoothing, often used in fMRI preprocessing pipelines, influences the mixture of BOLD signals. We propose concrete steps how to analyze fMRI BOLD data to allow inferences about the functional role of small subcortical nuclei like the subthalamic nucleus and substantia nigra.

Introduction

The subthalamic nucleus (STN) and substantia nigra (SN) are small subcortical nuclei in the basal ganglia [1]. Many cognitive neuroscience studies using BOLD functional magnetic resonance imaging (fMRI) have shown that the STN and SN are involved in a range of tasks such as response inhibition [2–4], conflict processing [5], force production [6,7], working memory [8,9], and the adjustment of global and selective response thresholds [10] (Table 1). While several studies have shown the involvement of either the STN or the SN in tasks such as the stop-signal task or Simon task, several neurocomputational models make distinct functional predictions for these nuclei (e.g.[11,12]). For instance, Frank et al. [12,13] propose that the STN acts as a general brake, whereas the SN, through the release of dopamine, is activated by the correct

Table 1. Literature overview of BOLD fMRI STN and SN studies.

Author	Task	Age	Tesla	fMRI resolution (mm)	voxel size (mm^3)	FWHM (mm)	Structure	Definition of ROI	MNI peak coordinate		
									x	y	z
[53]	Feedback-driven classification-learning	20–33	3	3.125x3.125x6*	58.59	8	SN/VTA	Search space: 15mm3 sphere (0,-15,-9)	-6	-21	-9
[14]	Stop-signal paradigm	29.2 (4.5)	3	3.125x3.125x4	39.06	5	STN	ROI: 10mm3 box (10,-15,-5)	8	-20	-4
							STN		6	-18	-2
							STN		10	-14	-4
							STN		14	-18	-4
		23.8 (3.7)		1.56x1.56x3	7.30	2	STN	M.S. TSE sequence	N.S.	N.S.	N.S.
[54]	Stop-signal paradigm	28.1 (4.1)	3	3.125x3.125x4	39.06	5	STN	ROI: 10mm3 box (10,-15,-5)	6	-18	-4
							STN		8	-16	-6
							STN		14	-8	-4
							STN		10	-14	-4
[36]	Resting State	63.2 (8.7)	3	3x3x3*	27	5	STN	M.S. EPI sequence of 2 axial slices (z: –6 & –8)	-12	-14	-8
							STN		-14	-8	-6
[5]	Counting stroop	10.2 (0.8)	1,5	3.36x3.36x4	45.16	12	SN	Talairach atlas	-11,92	-19,31	-8,07
	Go/No-go		1,5	3.36x3.36x4	45.16	12	SN	Talairach atlas	-2,28	-12,25	-13,42
[55]	Automated four-digit finger sequence	25.8 (4.7)	3	3.6x3.6x3.6	46.66	8	SN	Talairach atlas	-2,32	-19,15	-18,34
							SN	Talairach atlas	1,15	-18,85	-15,57
[4]	Stop-signal paradigm	24.5 (n. s.)	3	3x3x3.3*	27	4	SN	Sig. voxels in the SN region	10	-22	-20
			3	3x3x3	27	8	SN	Sig. voxels in the SN region	12	-24	-14
							STN	Sig. voxels in the STN region	10	-16	-2
[56]	Visual discrimination	26 (n.s.)	3	2x2x3.6	14.4	6	SN	Visual inspection on mean PD sequence	8	-20	-14
							SN		-6	-18	-16
[57]	Resting State	29.9 (n. s.)	3	1.56x1.56x3	7.3	3	STN	Talairach atlas	N.S.	N.S.	N.S.
[58]	Checker board	18–35	1,5	N.S.xN.S.x3*	-	8	SN		-10	-16	-10
	Cognitive color-word stroop		1,5	N.S.xN.S.x3*	-		SN	ROI: 8mm sphere on peak voxel	-12	-2	-8
[59]	Visual oddball	23.9 (4.2)	3	3x3x3.3*	29.7	4	SN/VTA	M.S. MT sequence	8	-20	-18
							SN/VTA	M.S. MT sequence	12	-18	-20
[37]	Visual oddball	65.3 (6.3)	3	3x3x3.3*	29.7	4	SN/VTA	M.S. MT sequence	0	-14	-12
[60]	Slot machine	33.7(1.8)	3	3.1x3.1x3	28.83	10	SN/VTA	Coordinates of Duzel et al. 2008	-8	-20	-14
						4	SN/VTA		-8	-18	-18
							SN/VTA		12	-16	-12

(*Continued*)

Table 1. (*Continued*)

Author	Task	Age	Tesla	fMRI resolution (mm)	voxel size (mm^3)	FWHM (mm)	Structure	Definition of ROI	MNI peak coordinate		
									x	y	z
							SN/VTA		-6	-18	-16
[61]	Three-stage retrospective revaluation	25 (5)	3	3.1x3.1x5*	48.05	8	SN	Pickatlas	14	-20	-5
							SN		-10	-18	-8
[15]	Motor task switching	25.2 (n. s.) / 67.9 (n.s.)	3	2.5x2.5x2.83*	17.69	10	STN	ROI: 10mm3 box (10,-15,-5)	10	-15	-5
[62]	AX-CPT	20–53	3	1.5x1.5x1.9	4.28	3	SN/VTA	Talairach atlas	-5,51	-11,1	-12,36
[63]	Sequential decision making	19–53	3	1.5x1.5x1.9	4.28	3	SN/VTA	M.S. PD sequence	-1,32	15,3	-17,28±
							SN/VTA	M.S. PD sequence	-3,5	17,32	-18,57±
							SN	M.S. PD sequence	13,75	22,59	-20,5±
[3]	Stop-signal paradigm	22–45	3	3.4x3.4x4	46.24	10	STN	AAL atlas	N.S.	N.S.	N.S.
[64]	Perceptual decision making	23.9 (n. s.)	3	3x3x3*	27	8	STN	N.S.	-15	-18	0
[65]	Perceptual decision making	25.3 (n. s.)	3	3x3x3*	27	8	STN	ROI: 10mm3 box (10,-15,-5)	10	-15	-5
[66]	Go/No-go	23 (1.72)	3	1.5x1.5x1.5	3.38	6	SN/VTA	M.S. MT sequence	8	-9	-10
							SN/VTA	M.S. MT sequence	-12	-19	-7
[67]	Go/No-go	23.3 (5)	3	1.5x1.5x1.5	3.38	6	SN/VTA	M.S. MT sequence	12	-18	-10
							SN/VTA	M.S. MT sequence	-7	-22	-14
							SN/VTA	M.S. MT sequence	7	-20	15±
[68]	Simon task	23 (3.9)	3	N.S.xN.S.x3.7*	-	8	SN/STN	ROI: 12 mm sphere (-10,-15,-5)	16	-8	-10
							STN		-14	-12	-6
[69]	Stop-signal paradigm	27.6 (5.5)	3	3.4x3.4x4	46.24	8	STN	Pickatlas	3	-25	-2
							STN		6	-13	-5
[70]	Simon task / Stop-signal paradigm	23.6 (n. s.)	3	2.3x2.3x3.3*	17.46	N.S.	STN	Anatomical ROI centered on 8,-9,-11	8	-9	-11
[71]	Nonaversive differential conditioning	23.3 (n. s.)	1,5	3x3x5	45	6	SN	Talairach atlas	-8,37	-15,78	-15,73
							SN	Talairach atlas	10,69	-24,87	-11,89
							SN	Talairach atlas	-8,34	-18,59	-9,99
							SN	Talairach atlas	10,67	-22,06	-17,63
[72]	Reward anticipation paradigm	25 (2.9)	3	3.5x3.5x3.5	42.88	6	SN/VTA	N.S.	9	-18	-18
							SN/VTA		9	-12	-18
							SN/VTA		15	-15	-9
[73]	Reward anticipation paradigm	24.7 (2.1)	3	1.5x1.5x2	4.5	3	SN	ROI: 2mm sphere on peak voxel	9	-19	-14
							SN		10	-19	-15
							SN		12	-17	-8

(*Continued*)

Table 1. (*Continued*)

Author	Task	Age	Tesla	fMRI resolution (mm)	voxel size (mm^3)	FWHM (mm)	Structure	Definition of ROI	MNI peak coordinate		
									x	y	z
[74]	Spatial attention	21.7 (3.2)	3	3x3x3	27	6	STN	ROI: 2mm sphere on peak voxel	8	-16	-6
							SN/VTA		4	-14	-12
							SN/VTA		-2	-16	-14
							SN/VTA		2	-20	-16
							SN/VTA		-4	-14	-12
							SN/VTA		4	-12	-12
[75]	Complex motor sequence	22.9 (3.9)	3	1.5x1.5x2.5	5.63	10	STN	Atlas by Yelnik et al. 2003	-13,62	-16,2	-4,57
							STN		-11,53	-12,11	-7,08
							STN		11,71	-12,05	-9,44
							STN		-11,53	-12,11	-7,08
							STN		15,94	-11,88	-7,26
							STN		11,71	-12,05	-9,44
[76]	Counting stroop task	10.2 (1.3)	1,5	N.S.xN.S.x4	-	N.S.	SN	-	-11,92	-19,31	-8,07
[77]	Motor task switching	24.5 (n. s.) / 25.3 (n.s.)	3	2.5x2.5x3.08*	19.25	10	STN	ROI: 10mm3 box (10,-15,-5)	8	-10	-8
							STN		-5	-10	-8
[10]	Task switching	23.4 (4.8)	1,5	4x4x4	64	8	STN	ROI: Forstmann et al. 2010 masks	N.S.	N.S.	N.S.
[78]	Complex motor	27.7 (2.4)	3	3.4x3.4x3.3*	38.15	6	STN	Talairach atlas	N.S.	N.S.	N.S.
[79]	Probability discount	26.6 (4.2)	3	2x2x3*	12	8	SN/VTA	Coordinates of Schott et al. 2006	6	-20	-10
							SN/VTA		-8	-16	-12
							SN/VTA		-10	-16	-12
[80]	Montreal card-sorting	23.4 (n. s.)	1,5	4.7x4.7x4.7	103.82	6	STN	Talairach atlas	-11,86	-24,32	-4,22
							STN		-9,81	-23,02	-13,35
							STN		14,03	-20,18	-7,31
[81]	Reward learning	26 (3)	3	3.1x3.1x5*	48.05	6	SN/VTA	N.S.	10	-8	-6
							SN/VTA		-4	-16	-6
							SN/VTA		-8	-20	-6
							SN/VTA		12	-22	-4
							SN/VTA		-8	-20	-8
							SN/VTA		14	-16	-6
							SN/VTA		8	-22	-8
[82]	Gambling	21.4 (n. s.)	3	3.28x3.28x3	32.28	8	STN	Talairach atlas	15,97	-18,05	-4,62
							SN		2,21	-18,78	-14,47
[83]	Force production	20–37	3	3.125x3.125x3	29.30	N.S.	STN	BGHAT template	-10,46	-14,14	-5,84
[84]	Stop-signal paradigm	22–45	3	3.4x3.4x4	46.24	6	STN	ROI: 10mm3 box (10,-15,-5)	-6	-21	-3
							STN		-6	-21	-3
							STN		9	-21	-6
							STN		-12	-12	-6

(*Continued*)

Table 1. (*Continued*)

Author	Task	Age	Tesla	fMRI resolution (mm)	voxel size (mm^3)	FWHM (mm)	Structure	Definition of ROI	MNI peak coordinate		
									x	y	z
							STN		12	-12	-3
							STN		-12	-12	-3
							STN		12	-12	-3
							STN		-12	-15	-3
							STN		12	-15	-9
[85]	Resting state	26 (5)	3	3.3x3.9x4*	51.48	0	STN	N.S.	N.S.	N.S.	N.S.
							SN	N.S.	N.S.	N.S.	N.S.
[86]	Associative memory	n.s. / 18–31	1,5	3.13x3.13x6*	58.78	8	SN	M.S. MT sequence	N.S.	N.S.	N.S.
[87]	Delayed monetary incentive task	22.8 (1.5)	3	3.5x3.5x2	24.50	6	SN/VTA	M.S. PD sequence	-7	-23	-18
[88]	Face scene association learning	18–24	3	3.125x3.125xN.S.	-	8	SN/VTA	ROI: 10mm3 sphere on peak voxel Adock et al. 2006	3	-18	-12
[7]	Force production	20–35	3	3.125x3.125x3	29.30	5	STN	Talairach atlas	-10,46	-14,14	-5,84
[6]	Force production	21–35	3	3.125x3.125x5	48.83	N.S.	STN	Talairach atlas	N.S.	N.S.	N.S.
[89]	Force production	21–35	3	3.125x3.125x3	29.30	0	STN	Talairach atlas	-10,46	-14,14	-5,84
[38]	Resting state	55.3 (n.s.)	3	4x4x5	80	8	STN	ICA	9	-11	-3
							STN	Talairach atlas	-9	-12	-3
							SN	ICA	-9	-18	-12
[90]	Reward anticipation	22.9 (3)	1,5	3.13x3.13x6*	58.78	8	SN	Talairach atlas	7,44	-22.1	-15.97
							SN		11,04	-19,39	-12,83
[91]	Novelty	24.5 (4)	3	3x3x3	27	4	SN/VTA	Talairach atlas	5,28	-23,17	-15,83
							SN		14	-24,75	-10,22
							STN		-7,6	-11,65	-6,67
[8]	Working memory paradigm	33.1 (10.7) / 28.8 (7.3)	1,5	3.4x3.4x4	46.24	2	SN	Pickatlas	-8	-16	-12
							SN		8	-16	-14
[9]	Working memory updating	28 (4.4)	3	3x3x3	27	4	SN/VTA	M.S. MT sequence	10	-12	-12

M.S. Manual segmentation, TSE: Turbo spin echo, PD proton-density weighted, MT: Magnetization transfer,

* a slice gap was used,

±: coordinates not displayed in Fig. 1. The age is given in the mean years if provided, otherwise the range is given. N.S. not specified.

doi:10.1371/journal.pone.0120572.t001

response and inhibits the incorrect response. However, the small size and close proximity of the STN to the SN, as well as to the surrounding brain structures, frustrates precise localization and makes it challenging to attribute the BOLD signal to either STN or SN, respectively. A common procedure is to place a box of 10x10x10 mm on a center coordinate in the STN and extract the mean BOLD fMRI signal in this box, to estimate the signal change in the STN [2,14,15]. Note that the volume of such a box is about 7.5 times larger than the average STN volume reported in the literature (1000 mm^3 as compared to a weighted average of 119.88 mm^3 and a weighted median of 131.75 mm^3 [16–29]. In combination with often-used

smoothing procedures, the signals originating from the STN and SN will get mixed, making it difficult to unequivocally attribute signal to either structure [30,31].

The goal of this study was to investigate the consistency of the coordinates found in fMRI studies on the STN and SN, summarize the methods employed in these studies, and assess the severity of the problems with localization and mixture of signals. In a first step, we conducted a comprehensive literature search to characterize the methods resulting in significant functional activation in the STN and SN. In a second step, the peak coordinates of the STN and SN derived from these studies were compared to the location of recently published probability STN and SN ultra-high resolution 7T MRI atlas [28]. Thirdly, using ultra-high resolution individual anatomical MRI masks, a simulation study was performed to test the influence of different smoothing kernels on the mixture of BOLD fMRI signals from both the STN and SN.

Materials and Methods

Selection of STN and SN BOLD fMRI studies

A comprehensive search for relevant neuroimaging studies in the field of BOLD fMRI studies including the STN and SN was carried out using Google scholar (http://scholar.google.com/). The main keywords utilized were 'fMRI + substantia nigra', 'fMRI + SN', 'fMRI + subthalamic nucleus', 'fMRI + STN', as well as all combinations of the aforementioned terms.

Based on the information contained in the abstracts of all the papers returned, empirical studies were selected to meet the following inclusion criteria: (1) Studies were published in peer-review English language journals between January 2000 and March 2014; (2) the studies used BOLD fMRI; (3) the studies reported a functional coordinate that could be attributed to either the SN or STN; and (4) the studies reported the location of activation as 3D coordinates in stereotactic space of Talairach or the Montreal Neurological Institute (MNI).

All empirical studies included were cross-referenced and all papers citing these empirical studies were searched, using the Google scholar citation index tool. The whole selection process was repeated for the newly obtained empirical papers until no new studies were found. This resulted in the inclusion of 52 papers (see Table 1).

All activation foci of the included studies that were originally reported in Talairach space were converted to the MNI stereotactic space using the Lancaster et al. transformation algorithm, which has been validated and shown to substantially reduce any bias between the two references spaces [32].

Probabilistic ultra-high resolution 7T MRI atlas maps

For analysis of the comparison between STN and SN coordinates reported in the literature (see Table 1), we used previously reported ultra-high resolution 7T MRI probability maps [28]. The probability maps are based on 30 participants (14 females) with a mean age of 24.2 year (SD 2.4). The STN and SN masks were manually segmented by two raters for each individual on 7T zoomed multi-echo 3D FLASH MRI data with an isotropic voxel size of 0.5 mm [33]. Only voxels rated by both raters as belonging to the STN or SN were included in further analyses. Note that no differentiation between the SN pars compacta and the pars reticulate were made because the voxel resolution and used scan sequence did not allow for identification of the two subparts. The individual masks were then linearly registered to MNI standard space and combined to create a probabilistic atlas. For more information regarding the segmentation, MRI scanning sequence, and registration procedure see [28,34]. The structural data can be found on http://www.nitrc.org/projects/atag_mri_scans/ and on http://dx.doi.org/10.5061/dryad.fb41s. The probabilistic masks can be found on http://www.nitrc.org/projects/atag.

Simulation study

A simulation study was performed to assess the amount of signal that originates from neighboring nuclei that can be introduced into a region of interest (ROI) by smoothing. Sixty STN and sixty SN masks (thirty masks in both hemispheres) from the ATAG (Atlas of The bAsal Ganglia) dataset [28] were used in a total of 60 simulations, all using one STN and one SN mask at a voxel resolution of 0.5 mm isotropic. It was assumed that every voxel in each mask contained a signal of unit strength. Then, smoothing kernels of different sizes were applied, and for every voxel and for every nucleus, the amount of signal in that voxel originating from that nucleus was determined. If the entire signal came from the same nucleus, the value was 1. If no signal from that nucleus reached that voxel, the value was 0. The sum of the signal strengths of the two nuclei in a voxel could never surpass 1.

We focused on the mixture of signal in the center voxel of both masks, to emulate a ROI study where the ROI would be placed in the best possible voxel according to the ground truth. This is a very optimistic scenario considering the difficulty of STN/SN localization as discussed earlier. For every center voxel, two quantities were computed:

$$\mathrm{mass}_{\mathrm{SN}} = \sum_{x}\sum_{y}\sum_{z} \exp\left(-\left(\frac{(x - x_{com})}{2\sigma^2} + \frac{(y - y_{com})}{2\sigma^2} + \frac{(z - z_{com})}{2\sigma^2}\right)\right) \mathrm{SN}_{\mathrm{m}}\mathrm{ask}[x, y, z]$$

and

$$\mathrm{mass}_{\mathrm{STN}} = \sum_{x}\sum_{y}\sum_{z} \exp\left(-\left(\frac{(x - x_{com})}{2\sigma^2} + \frac{(y - y_{com})}{2\sigma^2} + \frac{(z - z_{com})}{2\sigma^2}\right)\right) \mathrm{STN}_{\mathrm{m}}\mathrm{ask}[x, y, z]$$

corresponding to the amount of signal originating from the SN and the amount of signal originating from the STN.

$[x_{com},y_{com},z_{com}]$ is the coordinate of the center-of-mass of the mask-of-interest in millimeters.STN_mask[x,y,z] was either 1 or 0, corresponding to the coordinate [x,y,z] being in the STN or not, SN_mask[x,y,z] analogously for the SN. σ is the standard deviation of the Gaussian kernel, which can be calculated for a given FWHM (full width at half maximum) by using the following formula:

$$\sigma = \frac{\mathrm{FWHM}}{2\sqrt{2\ln 2}}$$

Results

Overview of functional MRI STN and SN studies

52 functional MRI studies were included in the present study (Table 1), published between 2003 and 2014. These studies employed for instance resting state, the stop-signal task, decision-making tasks including reward and outcome manipulations, and threshold adjustments in cognitive control tasks. Smoothing kernels ranged between 0 mm – 12 mm and data was collected on either 1.5 or 3T scanners. Note that not all studies report extensive methodological or procedural information, which limits the assessment of their anatomical specificity [35].

Table 2. Average deviation of reported coordinates from center of mass ATAG masks.

	N of reported coordinates (n of studies)	Distance in x	Distance in y	Distance in z	Total distance
Left hemisphere					
SN	12 (9)	1.0 (3.4)	0.5 (4.9)	0.6 (3.6)	5.6 (4.0)
SN/VTA	17 (11)	2.9 (2.8)	2.6 (11.8)	–0.3 (4.2)	9.1 (9.6)
STN	20 (12)	–0.9 (2.8)	–1.2 (4.4)	1.3 (2.8)	5.2 (3.3)
Right hemisphere					
SN	18 (10)	–0.9 (3.7)	–1.6 (11.1)	–1.8 (4.0)	8.9 (8.6)
SN/STN	1 (1)	5.5 (-)	8.2 (-)	2.2 (-)	10.1 (-)
SN/VTA	17 (11)	–2.6 (4.1)	–1.3 (4.5)	0.2 (3.8)	7.1 (2.6)
STN	17 (14)	–1.6 (2.9)	–3.7 (4.2)	3.0 (5.1)	7.3 (4.7)

Distance of reported MNI coordinates from the center of mass of the corresponding ATAG STN probabilistic mask (for STN coordinates) or ATAG SN probabilistic mask (for all other coordinates, "SN", "SN/STN" and "SN/VTA") in millimeters (standard deviation). A coordinate with a higher X-value lies more to the right. A coordinate with a higher Y-value lies more anterior. A coordinate with a higher Z-value lies more superior.

doi:10.1371/journal.pone.0120572.t002

STN and SN coordinates in MNI space compared to ultra-high resolution 7T atlas maps

The reported STN and SN-coordinates were compared to the center-of-mass coordinates of the previously published 7T MRI probabilistic masks [28]. Results are summarized in Table 2.

On average, reported STN activity coordinates lay 5.2 mm (left hemisphere, std. = 3.3) and 5.7 mm (right hemisphere, std. = 2.8) from the center-of-mass of the 7T MRI probabilistic mask. Several studies include older participants [15,36–38]). This might result in a mismatch between the reported coordinates and the probabilistic atlas because it is known that the STN shifts in lateral direction with age [29,39,40]. Note, however, that this lateral shift is smaller (on average 1.6 mm more lateral for elderly than for young participants [29]) compared to the standard deviation reported in the present study. The mismatch in location is predominantly observed in the dorsal-ventral and anterior-posterior direction such that the reported coordinates were on average 1.3 / 1.5 (left/right, std. = 2.8/2.5) mm more dorsal and 1.2 / 2.5 (left/right std. = 4.4/4.0) mm more anterior than the center-of-mass of the 7T probabilistic STN masks.

The left STN coordinates were on average 0.9 mm (std. = 2.8) more medial than the center-of-mask of the 7T MRI probabilistic mask, and the right STN coordinates lay on average 0.4 mm (std. = 3.2) more lateral. The average distance between the centers-of-mass of the SN and STN of the probabilistic masks is in the same order of magnitude as the distance between the average reported STN fMRI location and the actual STN center-of-mass (6.4 mm left, 6.7 mm right; std. = 0.7 / 0.7).

Reported SN activity coordinates were on average 5.6 (left hemisphere, std. = 4.0) and 8.9 (right hemisphere, std. = 8.6) mm away from the center of mass of the 7T MRI probabilistic mask. Shifts occurred in all three directions.

Fig. 1 shows coronal plots of the probabilistic maps with the reported coordinates rendered onto them. Only coordinates that lay within the MNI coordinate range of x: 18,-18 / z: 0,-21 / y: –2,-25 were plotted. The coordinates that fell outside of this range are marked in Table 1.

The average FWHM size of the smoothing kernel was 6.3 mm (median 6 mm). The 8 mm FWHM smoothing kernel was used most frequently (16 out of 52 studies: see Fig. 2 for the relative size of the kernels used compared to the STN and SN). There was no relationship between the nucleus of interest and the smoothing kernel used.

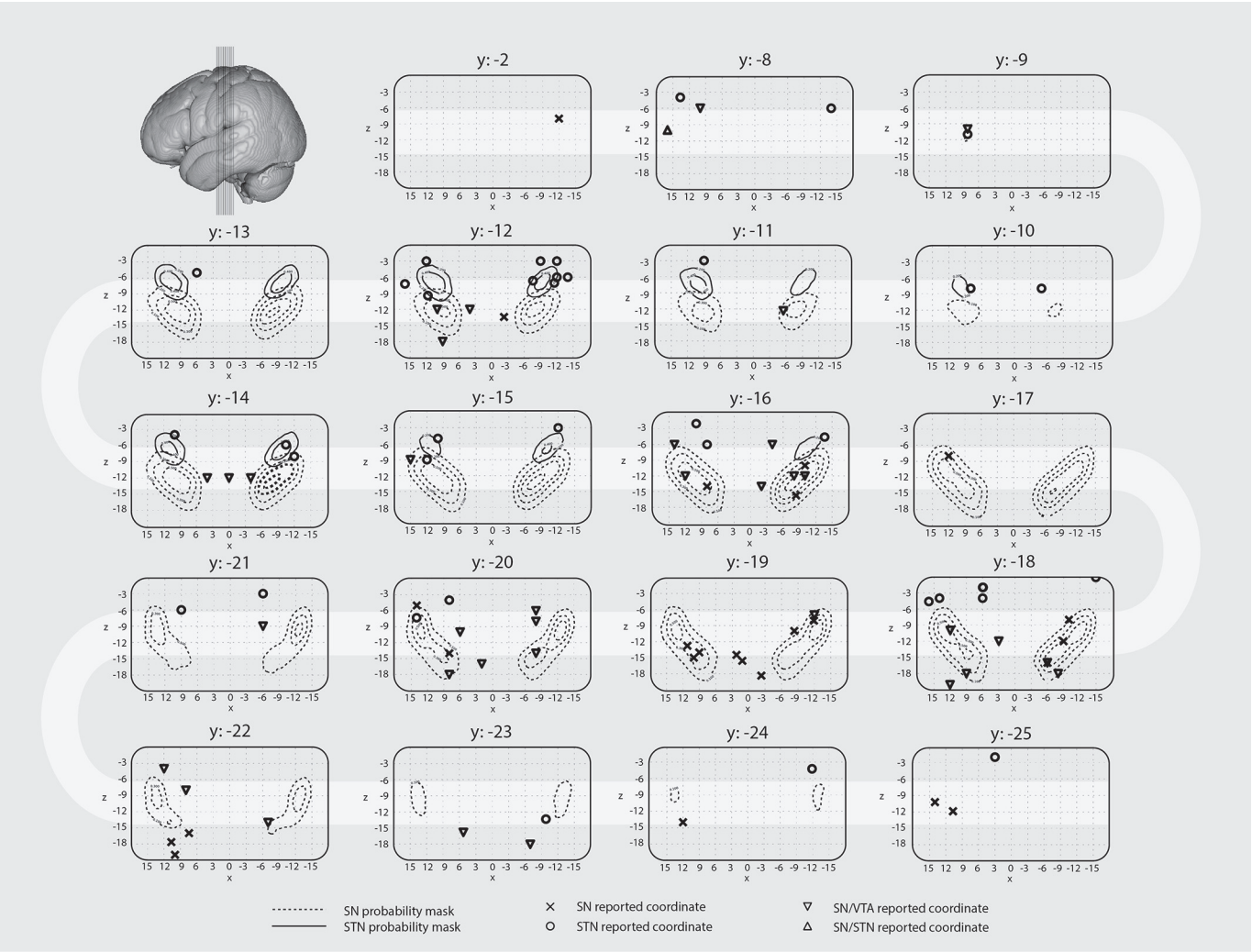

Fig 1. Location of individual peak coordinates of the STN and SN. Coronal slices in anterior to posterior direction are displayed together with functional coordinates of the STN, SN, SN/VTA, and SN/STN as reported in Table 1. Overlaid onto these coordinates is the probabilistic atlas of the STN and SN. The isolines reflect the percentage overlap across the 30 young subjects taken from Keuken et al. [28]. The outermost isolines reflects a 10% probability of containing the SN at the population level, the more inner lines represent 30%, 50%, and 70% probability of containing the SN. The outermost isolines for the STN reflects a probability of 20% containing the STN, the inner line represent 40% probability of containing the STN. The grid size corresponds to a voxel size of 3x3 mm. All coordinates are in MNI standard space.

doi:10.1371/journal.pone.0120572.g001

To test for any spatial biases introduced by smoothing, as reported by e.g. Sacchet et al., [41] for the nucleus accumbens, MNI coordinates were correlated with the size of the smoothing kernel employed. No correlations were found except for the SN ($r(45) = .83$, $p < 0.05$, uncorrected), which lay more superior as a function of a larger smoothing kernel. The majority of studies (47 out of the 52) reported the voxel resolution. The voxel resolution was on average 34 mm^3 (median 32 mm^3, std. = 21 mm, range 3.4–103.8 mm).

Simulation of effects of smoothing on subcortical fMRI activations

Fig. 3 qualitatively illustrates the effect of an 8 mm FWHM smoothing kernel on individual masks of the left and right STN and SN. The result shows that signal originating from each nucleus spreads widely, also across its neighbor's boundaries (Fig. 4).

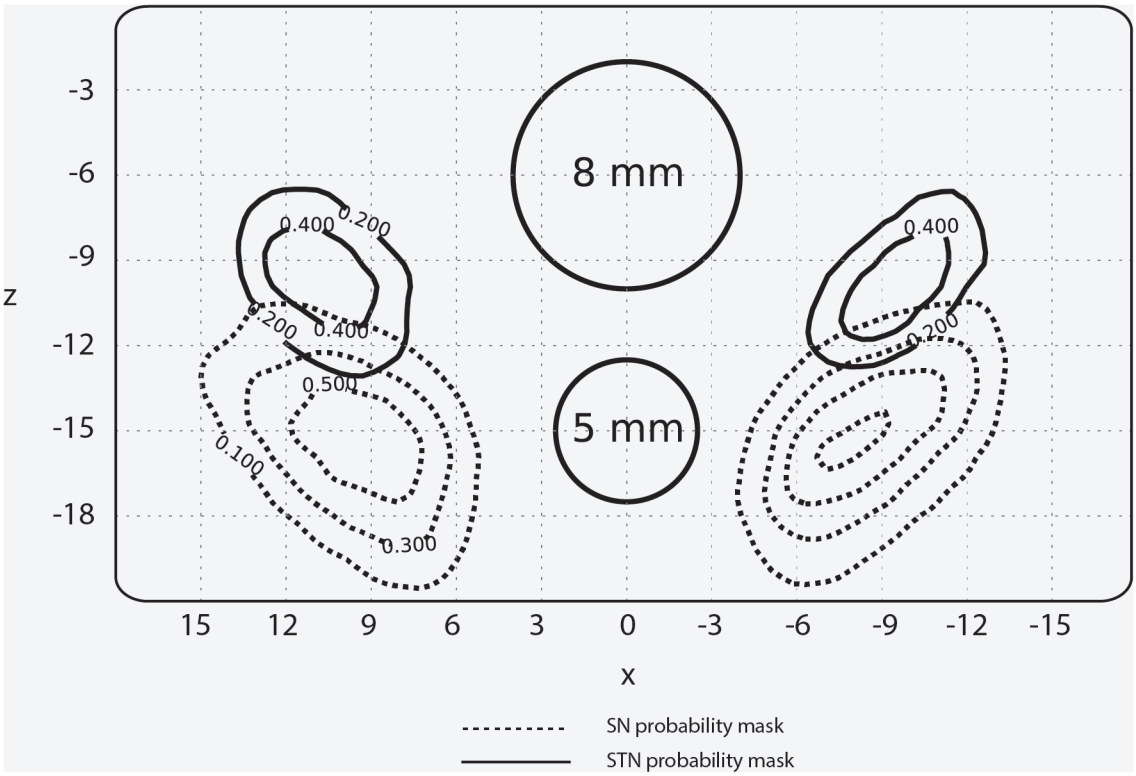

Fig 2. Relative size of a standard FWHM diameter compared to the STN and SN. A zoomed-in coronal slice (MNI y-coordinate: –14) showing the STN and SN. Two circles are shown in the middle to indicate the diameter of 2 frequently used FWHM smoothing kernels. The isolines reflect the percentage overlap across the 30 young subjects taken from Keuken et al.[28].

doi:10.1371/journal.pone.0120572.g002

When no smoothing was applied, the signal in the center voxel of both SN and STN originated completely from the nucleus of its location. When a 4 mm FWHM smoothing kernel was used, 30% of the signal in the center voxel of the STN was found to originate from outside the STN and SN, while ten percent originated from the SN and 60% from the STN itself. With an often-used 8 mm FWHM smoothing kernel, 75% of the signal in the center voxel of the STN mask originated from outside the STN and SN. Ten percent originated from the SN and only 15% from the STN itself. For this simulation, the strength of the STN signal in the center voxel was taken to be similar in size to the signal originating from the SN. Note that the results would vary if different signal strengths in both nuclei were assumed. However, the precise ratios have little effect on this finding. Importantly, this simulation shows that with large smoothing kernels it becomes impossible to disentangle the origin of the measured signal, even when focusing on the most central voxel. In empirical fMRI studies this is an unlikely scenario, because the voxel resolution is at an average of 34 mm3, instead of the 0.064 mm3 (0.4 mm isotropic) used here. In sum, the mixing of signals is likely to be substantially worse in empirical fMRI studies compared to this simulation study.

Discussion

In the present study we show that there is large variability in previously reported fMRI coordinates attributed to the STN and SN. We also show a discrepancy between individual coordinates of empirical studies and probabilistic atlas maps derived from ultra-high resolution 7T MRI [28]. The resolution of the fMRI sequences used in the studies we included was usually

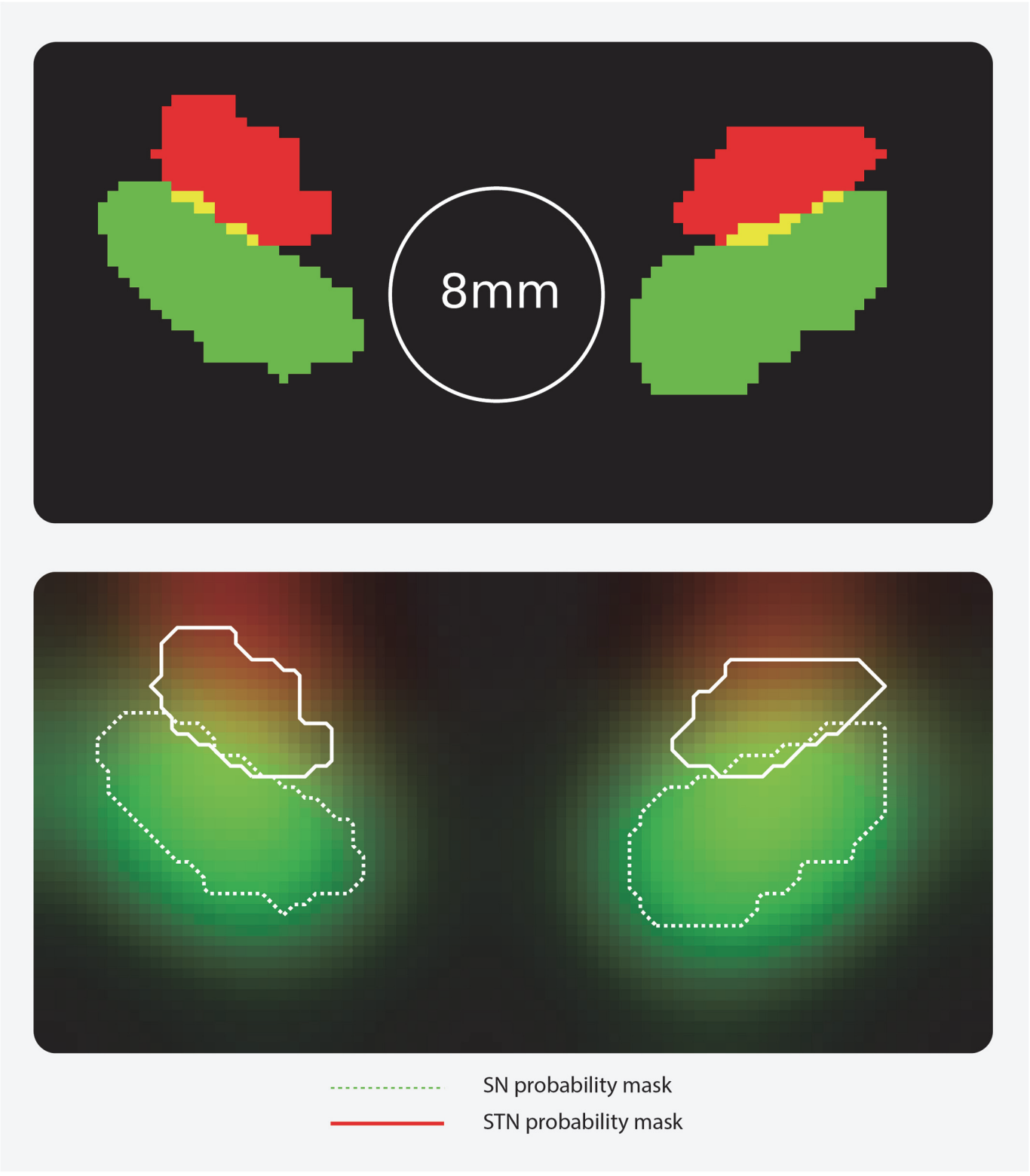

Fig 3. Illustration of effect of smoothing on mixture of BOLD signals between SN and STN. Four binary, individual masks are displayed of one representative participant smoothed with an 8 mm FWHM smoothing kernel.

doi:10.1371/journal.pone.0120572.g003

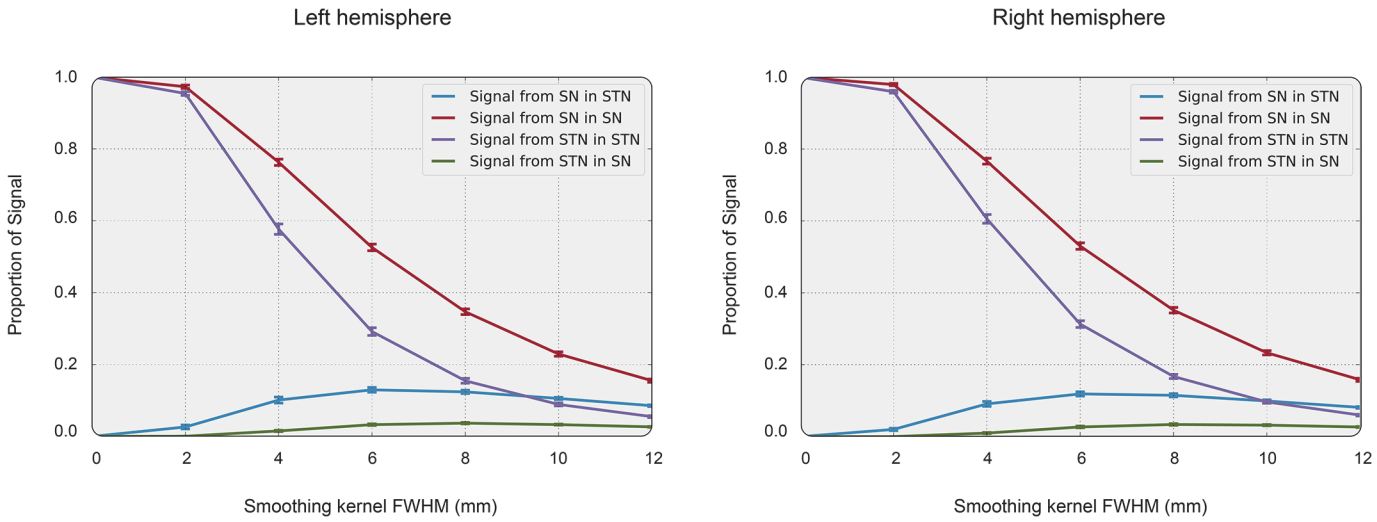

Fig 4. Simulation results: Effect of smoothing on mixture of BOLD signals between SN and STN. Summary of the smoothing simulation study. For both hemispheres, in 30 subjects taken from Keuken et al. [28], the effect of smoothing on the mixing of signals in STN and SN in their respective center voxels was estimated. The lines show the amount of signal for different source-destination pairs of STN and SN as a function of smoothing kernel size. When no smoothing is applied, all signal in the SN originates from SN and all signal in STN originates from the STN. When more smoothing is applied, the amount of signal originating from the nucleus that is measured sharply decreases, and within the STN the amount of signal from the SN becomes equal in size to the signal originating from the STN itself.

doi:10.1371/journal.pone.0120572.g004

low compared to the size of the nuclei of interest. The average voxel resolution was 34 mm^3 (median 32 mm^3; std 21 mm^3). Over the past years, the voxel resolution has also increased on 3T scanners. For all studies published since 2010 on 3T, mean voxel size was 22 mm^3 (median 23 mm^3; std 18 mm^3). There is a significant correlation between year-of-publication and voxel size ($r(115) = -0.31$, $p<0.001$). However, half of the studies published in 2013 and later ($n = 9$) still use a coarse voxel resolution; on average they used a resolution of 24 mm^3 (median 27 mm^3, std 20 mm^3), which results in only approximately 5 voxels covering the STN.

The simulation results reveal that when smoothing kernels of commonly used sizes are applied, the amount of signal from neighboring nuclei that get smoothed into a region of interest is of similar size as the signal from the region itself. This is particularly important when analyzing data from a small nucleus such as the STN, which borders the larger SN.

These results add empirical data to the recent discussion about smoothing in functional neuroimaging. Stelzer et al. [31] suggested that smoothing fMRI data should be abandoned altogether, because it (1) causes incorrect estimation of the true spatial extent of brain activation, (2) blurs away signals of limited spatial extent, and (3) frustrates the detection of low-intensity signals in the vicinity of non-active tissue. Our results illustrate quantitatively how large these effects can be, specifically for subcortical nuclei: we show that reported MNI coordinates largely non-overlap with anatomical masks (point 1) and that smoothing can induce substantial mixing with signal from outside the nucleus (point 2 and 3).

The use of smoothing can increase the signal-to-noise ratio in fMRI when the signal is more spatially correlated than the noise on the scale of the smoothing kernel employed. However, in the case of subcortical nuclei, the used smoothing kernels are often too large and mix in signal and noise from neighbouring structures. Yoon et al. [8] provide an empirical example of the influence of kernel size in their supplemental information: the activity in the SN only reached a significance threshold when a smoothing kernel with a very minor FWHM of 2 mm was employed. When a smoothing kernel with an FWHM of 8 mm was used, the effect disappeared. Because the voxel size of this study was rather large, 3.4x4x4 mm, the effect of a 2 mm

smoothing kernel was negligible and could have been abandoned altogether. When one applies such a relatively large smoothing kernel to data of such a relatively coarse resolution, the amount of signal in a voxel in the smoothed image originating from outside this voxel is less than 0.2% (See http://nbviewer.ipython.org/gist/Gilles86/0c093962de8cf05f76c8). The results by Yoon et al. thus clearly show that smoothing is not necessary to find significant effects in the substantia nigra region, even with 1.5T [8].

It has been suggested that a lack of spatial resolution and anatomical specificity could be overcome by using unsupervised clustering algorithms such as principal component analysis (PCA; [42]) or independent component analysis (ICA; [42]). These methods might 'detect' the nucleus of interest by exploiting the different covariance structures of the BOLD signal in different nuclei. We think, however, that such an approach is not appropriate. First and foremost, it assumes that the task-related BOLD activity in the STN and SN are uncorrelated. This is highly unlikely because both nuclei are part of the same functional networks, e.g., the basal ganglia motor control loops. Secondly, even if the signal could be separated to some extent, there is no objective way of finding out which cluster component belongs to which nucleus and to which extent they account for only one nucleus. Third, independent components might represent non-BOLD signals such as physiological noise. Fourth, the most adequate procedure of defining the actual signal of the nucleus of interest by means of, e.g. a demixing matrix (e.g., [43] or a Gaussian sphere [44]) remains elusive.

Therefore we suggest that during functional imaging of small subcortical nuclei, standard smoothing strategies should be avoided altogether. More complex, adaptive smoothing approaches [45] might be useful, but analysis protocols that do not require smoothing should be preferred. A-priori ROI analyses [46] do not require smoothing, nor do whole-brain univariate analysis approaches that make use of False Discovery Rate (FDR) as multiple comparison correction, as well as multivariate analysis strategies [31,47].

Concretely, we propose an approach that maximizes both anatomical specificity and signal-to-noise. Researchers are advised to use individual anatomical masks based on an appropriate MR contrast (i.e., $T2^*$ or quantitative susceptibility mapping (QSM)) that allows for detailed visibility and segmentation of the structures of interest (see, e.g., [27–29,48–50]). When individual segmentation is not feasible, researchers can use probabilistic atlas maps, as provided for the STN and SN in [27–29]. If the research question does not focus on anatomical patterns within the nucleus itself, the mean signal across all voxels in the nucleus can be analysed. This maximizes SNR and removes both the multiple comparisons problem, as well as the need for registration to a standard space. When different activation patterns within the nucleus are expected, a voxel-wise analysis within the anatomical mask can be computed.

Given the variability in reported coordinates and smoothing, one may question the validity of earlier fMRI findings in the STN/SN. It is important to note that studies with Parkinson Disease patients using deep-brain stimulation (DBS) [51] or lesioning of the STN [52] deliver important causal evidence for the functional role of the STN in motor control. fMRI studies that report BOLD activity in motor control paradigms are thus likely to be sensitive to actual task involvement. However, we believe that caution is warranted in interpreting the anatomical specificity of these findings. Especially interpreting findings from studies that 1) use smoothing kernels with a FWHM of more than 4 mm, 2) do not use anatomical masks that are based on individual anatomy, either individually segmented or based on a population probabilistic map like the ATAG dataset [28], and finally, 3) use voxel resolutions that are in the same order of magnitude as the nucleus itself.

In sum, the present study provides evidence for the importance of accounting for individual anatomy when attempting to understand the functional role of small subcortical areas such as the STN and SN. Moreover, the combination of ultra-high resolution fMRI with a very high

voxel resolution and zoomed-in acquisition protocols will help to unmix signals arising from small subcortical structures in very close proximity. Finally, the simulation results indicate that spatial smoothing should be avoided when one values anatomical specificity of functional neuroimaging results.

Acknowledgments

We would like to thank Robert Turner, Andreas Schaefer, Pierre-Louis Bazin, as well as Siemens Medical Solutions. The work was supported by a starter grant from the European Research Council (ERC) to Birte U. Forstmann.

Author Contributions

Conceived and designed the experiments: BF GdH MK. Performed the experiments: BF GdH MK. Analyzed the data: BF GdH MK. Contributed reagents/materials/analysis tools: BF GdH MK. Wrote the paper: BF GdH MK.

References

1. Marani E, Heida T, Lakke E, Usunoff K. The Subthalamic Nucleus. Berlin: Springer, 2008.
2. Aron A. The neural basis of inhibition in cognitive control. The Neuroscientist 2007; 13: 214. PMID: 17519365
3. Duann JR, Ide JS, Luo X, Li CSR. Functional Connectivity Delineates Distinct Roles of the Inferior Frontal Cortex and Presupplementary Motor Area in Stop Signal Inhibition. Journal of Neuroscience 2009; 29: 10171–10179. doi: 10.1523/JNEUROSCI.1300-09.2009 PMID: 19675251
4. Boehler CN, Bunzeck N, Krebs RM, Noesselt T, Schoenfeld MA, Heinze H-J, et al. Substantia Nigra Activity Level Predicts Trial-to-Trial Adjustments in Cognitive Control. Journal of cognitive neuroscience 2011; 23: 362–373. doi: 10.1162/0898929041502779 PMID: 20465358
5. Beauregard M, Lévesque J. Functional Magnetic Resonance Imaging Investigation of the Effects of Neurofeedback Training on the Neural Bases of Selective Attention and Response Inhibition in Children with Attention-Deficit/Hyperactivity Disorder. Appl Psychophysiol Biofeedback 2006; 31: 3–20. doi: 10.1007/s10484-006–9001-y PMID: 16552626
6. Vaillancourt DE, Mayka MA, Thulborn KR, Corcos DM. Subthalamic nucleus and internal globus pallidus scale with the rate of change of force production in humans. NeuroImage 2004; 23: 175–186. doi: 10.1016/j.neuroimage.2004.04.040 PMID: 15325364
7. Spraker MB, Yu H, Corcos DM, Vaillancourt DE. Role of individual basal ganglia nuclei in force amplitude generation. Journal of Neurophysiology 2007; 98: 821. PMID: 17567775
8. Yoon JH, Minzenberg MJ, Raouf S, Esposito MDX, Carter CS. Impaired Prefrontal-Basal Ganglia FunctionalConnectivity and Substantia Nigra Hyperactivityin Schizophrenia. Biol Psychiatry 2013; 74: 122–129. doi: 10.1016/j.biopsych.2012.11.018 PMID: 23290498
9. Yu Y, FitzGerald THB, Friston KJ. Working Memory and Anticipatory Set Modulate Midbrain and Putamen Activity. Journal of Neuroscience 2013; 33: 14040–14047. doi: 10.1523/JNEUROSCI.1176-13.2013 PMID: 23986240
10. Mansfield EL, Karayanidis F, Jamadar S, Heathcote A, Forstmann BU. Adjustments of Response Threshold during Task Switching: A Model-Based Functional Magnetic Resonance Imaging Study. Journal of Neuroscience 2011; 31: 14688–14692. doi: 10.1523/JNEUROSCI.2390-11.2011 PMID: 21994385
11. Bogacz R, Gurney K. The basal ganglia and cortex implement optimal decision making between alternative actions. Neural Computation 2007; 19: 442–477. PMID: 17206871
12. Frank MJ, Samanta J, Moustafa AA, Sherman SJ. Hold your horses: impulsivity, deep brain stimulation, and medication in parkinsonism. Science 2007; 318: 1309–1312. PMID: 17962524
13. Frank MJ. Dynamic dopamine modulation in the basal ganglia: a neurocomputational account of cognitive deficits in medicated and nonmedicated Parkinsonism. Journal of cognitive neuroscience 2005; 17: 51–72. PMID: 15701239
14. Aron AR. Cortical and Subcortical Contributions to Stop Signal Response Inhibition: Role of the Subthalamic Nucleus. Journal of Neuroscience 2006; 26: 2424–2433. doi: 10.1523/JNEUROSCI.4682-05.2006 PMID: 16510720

15. Coxon JP, Goble DJ, Van Impe A, De Vos J, Wenderoth N, Swinnen SP. Reduced Basal Ganglia Function When Elderly Switch between Coordinated Movement Patterns. Cerebral Cortex 2010; 20: 2368–2379. doi: 10.1093/cercor/bhp306 PMID: 20080932

16. Bonin von G, Shariff GA. Extrapyramidal nuclei among mammals; a quantitative study. J Comp Neurol 1951; 94: 427–438. doi: 10.1002/cne.900940306 PMID: 14850586

17. Fussenich M. Vergleichend anatomische studien uber den nucleus subthalamicus (corpus Luys) bei primaten.1967: 1–55.

18. Hardman CD, Halliday GM, McRitchie DA, Morris JG. The subthalamic nucleus in Parkinson's disease and progressive supranuclear palsy. J Neuropathol Exp Neurol 1997; 56: 132–142. PMID: 9034366

19. Weiss M, Alkemade A, Keuken MC, Müller-Axt C, Geyer S, Turner, R, et al. Spatial normalization of ultrahigh resolution 7 T magnetic resonance imaging data of the postmortem human subthalamic nucleus: a multistage approach. Brain Struct Funct. 2014.

20. Lange H, Thörner G, Hopf A, Schröder KF. Morphometric studies of the neuropathological changes in choreatic diseases. J Neurol Sci 1976; 28: 401–425. PMID: 133209

21. Yelnik J. Functional anatomy of the basal ganglia. Movement Disorders 2002; 17: S15–S21. PMID: 11948751

22. Hardman C, Henderson J, Finkelstein D, Horne M, Paxinos G, Halliday GM. Comparison of the basal ganglia in rats, marmosets, macaques, baboons, and humans: volume and neuronal number for the output, internal relay, and striatal modulating nuclei. J Comp Neurol 2002; 445: 238–255. PMID: 11920704

23. Lévesque J, Parent A. GABAergic interneurons in human subthalamic nucleus. Movement Disorders 2005; 20: 574–584. PMID: 15645534

24. Wei-gao S, Hai-yang W, Zhi-guo L, Hong S, Xiao-guang C, Yi-li FU, et al. Stereotactic localization and visualization of the subthalamic nucleus. Chinese Medical Journal 2009; 122: 2438–2443. PMID: 20079156

25. Colpan ME, Slavin KV. Subthalamic and red nucleus volumes in patients with Parkinsons disease: Do they change with disease progression? Parkinsonism and realted Disorders 2010; 16: 398–403. doi: 10.1016/j.parkreldis.2010.03.008 PMID: 20452266

26. Lenglet C, Abosch A, Yacoub E, De Martino F, Sapiro G, Harel N. Comprehensive in vivo Mapping of the Human Basal Ganglia and Thalamic Connectome in Individuals Using 7T MRI. PloS one 2012; 7: e29153. doi: 10.1371/journal.pone.0029153.t001 PMID: 22235267

27. Forstmann BU, Keuken MC, Jahfari S, Bazin PL, Neumann N, Schafer A, et al. Cortico-subthalamic white matter tract strength predict interindividual efficacy in stopping a motor response. NeuroImage 2012; 60: 370–375. doi: 10.1016/j.neuroimage.2011.12.044 PMID: 22227131

28. Keuken MC, Bazin PL, Crown L, Hootsmans J, Laufer A, Muller-Axt C, et al. Quantifying inter-individual anatomical variability in the subcortex using 7T structural MRI. NeuroImage 2014; 94: 1–7. doi: 10.1016/j.neuroimage.2014.03.032 PMID: 24642284

29. Keuken MC, Bazin PL, Schafer A, Neumann J, Turner R, Forstmann BU. Ultra-High 7T MRI of Structural Age-Related Changes of the Subthalamic Nucleus. Journal of Neuroscience 2013; 33: 4896–4900. doi: 10.1523/JNEUROSCI.3241-12.2013 PMID: 23486960

30. Turner R. Where matters: new approaches to brain analysis. In: Geyer S, Turner R, editors. Microstructural parcellation of the human cerebral cortex. Heidelberg: Springer 2013.

31. Stelzer J, Lohmann G, Mueller K, Buschmann T, Turner R. Deficient Approaches to Human Neuroimaging. Name: Frontiers in Human Neuroscience 2014; 8: 462. doi: 10.3389/fnhum.2014.00462/abstract PMID: 25071503

32. Lancaster JL, Tordesillas-Gutiérrez D, Martinez M, Salinas F, Evans A, Zilles K, et al. Bias between MNI and Talairach coordinates analyzed using the ICBM-152 brain template. Hum Brain Mapp 2007; 28: 1194–1205. doi: 10.1002/hbm.20345 PMID: 17266101

33. Haase A, Frahm J, Matthaei D, Hanicke W, Merboldt KD. FLASH imaging. Rapid NMR imaging using low flip-angle pulses. Journal of Magnetic Resonance 1986; 67: 258–266.

34. Forstmann BU, Keuken MC, Schäfer A, Bazin PL, Alkemade A, Turner, R. Multi-modal ultra-high resolution structural 7-Tesla MRI data repository. Scientific Data 2014.

35. Poldrack R, Fletcher P, Henson R, Worsley K, Brett M, Nichols TE. Guidelines for reporting an fMRI study. NeuroImage 2008; 40: 409–414. doi: 10.1016/j.neuroimage.2007.11.048 PMID: 18191585

36. Baudrexel S, Witte T, Seifried C, Wegner von F, Beissner F, Klein JC, et al. Resting state fMRI reveals increased subthalamic nucleus–motor cortex connectivity in Parkinson's disease. NeuroImage 2011; 55: 1728–1738. doi: 10.1016/j.neuroimage.2011.01.017 PMID: 21255661

37. Bunzeck N, Schutze H, Stallforth S, Kaufmann J, Duzel S, Heinze HJ, et al. Mesolimbic Novelty Processing in Older Adults. Cerebral Cortex 2007; 17: 2940–2948. doi: 10.1093/cercor/bhm020 PMID: 17383999

38. Wen X, Yao L, Fan T, Wu X, Liu J. The spatial pattern of basal ganglia network: A resting state fMRI study. IEEE. 2012;43–46.

39. Dunnen Den WF, Staal MJ. Anatomical alterations of the subthalamic nucleus in relation to age: A postmortem study. Movement Disorders 2005; 20: 893–898. doi: 10.1002/mds.20417 PMID: 15809991

40. Kitajima M, Korogi Y, Kakeda S, Moriya J, Ohnari N, Sato T, et al. Human subthalamic nucleus: evaluation with high-resolution MR imaging at 3.0 T. Neuroradiology 2008; 50: 675–681. doi: 10.1007/s00234-008-0388-4 PMID: 18443775

41. Sacchet MD, Knutson B. Spatial smoothing systematically biases the localization of reward-related brain activity. NeuroImage 2013; 66: 270–277. doi: 10.1016/j.neuroimage.2012.10.056 PMID: 23110886

42. Bishop CM. Pattern Recognition and Machine Learning (Information Science and Statistics). New York: Springer Verlag 2006.

43. van Maanen L, Brown SD, Eichele T, Wagenmakers E-J, Ho T, Serences J, et al. Neural Correlates of Trial-to-Trial Fluctuations in Response Caution. Journal of Neuroscience 2011; 31: 17488–17495. doi: 10.1523/JNEUROSCI.2924-11.2011 PMID: 22131410

44. Erika-Florence M, Leech R, Hampshire A. A functional network perspective on response inhibition and attentional control. Nature Communications 2014; 5: 1–12. doi: 10.1038/ncomms5073.

45. Tabelow K, Piëch V, Polzehl J, Voss HU. High-resolution fMRI: Overcoming the signal-to-noise problem. J Neurosci Methods 2009; 178: 357–365. doi: 10.1016/j.jneumeth.2008.12.011 PMID: 19135087

46. Poldrack RA. Region of interest analysis for fMRI. Social Cognitive and Affective Neuroscience 2006; 2: 67–70. doi: 10.1093/scan/nsm006.

47. O'Toole AJ, Jiang F, Abdi H, Pénard N, Dunlop JP, Parent MA. Theoretical, statistical, and practical perspectives on pattern-based classification approaches to the analysis of functional neuroimaging data. Journal of cognitive neuroscience 2007; 19: 1735–1752. PMID: 17958478

48. Forstmann BU, Anwander A, Schafer A, Neumann J, Brown S, Wagenmakers E-J, et al. Cortico-striatal connections predict control over speed and accuracy in perceptual decision making. Proceedings of the National Academy of Sciences 2010; 107: 15916–15920. doi: 10.1073/pnas.1004932107 PMID: 20733082

49. Lefranc M, Derrey S, Merle P, Tir M, Constans J-M, Montpellier D, et al. High-Resolution 3-Dimensional T2*-Weighted Angiography (HR 3-D SWAN). Neurosurgery 2014; 74: 615–627. doi: 10.1227/NEU.0000000000000319 PMID: 24535261

50. Hollander G, Keuken MC, Bazin PL, Weiss, M, Neumann, J, Reimann, K, et al. A gradual increase of iron toward the medial-inferior tip of the subthalamic nucleus. Hum Brain Mapp 2014. doi: 10.1002/hbm.22485.

51. Cavanagh JF, Wiecki TV, Cohen MX, Figueroa CM, Samanta J, Sherman SJ, et al. Subthalamic nucleus stimulation reverses mediofrontal influence over decision threshold. Nature neuroscience 2011; 14: 1462–1467. doi: 10.1038/nn.2925 PMID: 21946325

52. Jahanshahi M. Effects of deep brain stimulation of the subthalamic nucleus on inhibitory and executive control over prepotent responses in Parkinson's disease. Frontiers in systems neuroscience 2013; 7. doi: 10.3389/fnsys.2013.00118/abstract.

53. Aron AR. Human Midbrain Sensitivity to Cognitive Feedback and Uncertainty During Classification Learning. Journal of Neurophysiology 2004; 92: 1144–1152. doi: 10.1152/jn.01209.2003 PMID: 15014103

54. Aron AR, Behrens TE, Smith S, Frank MJ, Poldrack RA.Triangulating a Cognitive Control Network Using Diffusion-Weighted Magnetic Resonance Imaging (MRI) and Functional MRI. Journal of Neuroscience 2007; 27: 3743–3752. doi: 10.1523/JNEUROSCI.0519-07.2007 PMID: 17409238

55. Boecker H, Jankowski J, Ditter P, Scheef L. A role of the basal ganglia and midbrain nuclei for initiation of motor sequences. NeuroImage 2008; 39: 1356–1369. doi: 10.1016/j.neuroimage.2007.09.069 PMID: 18024158

56. Boehler CN, Hopf JM, Krebs RM, Stoppel CM, Schoenfeld MA, Heinze HJ, et al. Task-Load-Dependent Activation of Dopaminergic Midbrain Areas in the Absence of Reward. Journal of Neuroscience 2011; 31: 4955–4961. doi: 10.1523/JNEUROSCI.4845-10.2011 PMID: 21451034

57. Brunenberg EJL, Moeskops P, Backes WH, Pollo C, Cammoun L, Vilanova A, et al. Structural and Resting State Functional Connectivity of the Subthalamic Nucleus: Identification of Motor STN Parts and the Hyperdirect Pathway. PloS one 2012; 7: e39061. doi: 10.1371/journal.pone.0039061.t003 PMID: 22768059

58. Brydon L, Harrison NA, Walker C, Steptoe A, Critchley HD. Peripheral Inflammation is Associated with Altered Substantia Nigra Activity and Psychomotor Slowing in Humans. Biol Psychiatry 2008; 63: 1022–1029. doi: 10.1016/j.biopsych.2007.12.007 PMID: 18242584

59. Bunzeck N, Düzel E.Absolute Coding of Stimulus Novelty in the Human Substantia Nigra/VTA. Neuron 2006; 51: 369–379. doi: 10.1016/j.neuron.2006.06.021 PMID: 16880131

60. Chase HW, Clark L. Gambling Severity Predicts Midbrain Response to Near-Miss Outcomes. Journal of Neuroscience 2010; 30: 6180–6187. doi: 10.1523/JNEUROSCI.5758-09.2010 PMID: 20445043

61. Corlett PR, Aitken MR, Dickinson A, Shanks DR, Honey GD, Honey RAE, et al. Prediction error during retrospective revaluation of causal associations in humans: fMRI evidence in favor of an associative model of learning. Neuron 2004; 44: 877–888. PMID: 15572117

62. D'Ardenne K, Eshel N, Luka J, Lenartowicz A, Nystrom LE, Cohen JD. Role of prefrontal cortex and the midbrain dopamine system in working memory updating. Proc Natl Acad Sci USA 2012; 109: 19900–19909. doi: 10.1073/pnas.1116727109/-/DCSupplemental PMID: 23086162

63. D'Ardenne K, Lohrenz T, Bartley KA, Montague PR. Computational heterogeneity in the human mesencephalic dopamine system. Cogn Affect Behav Neurosci 2013; 13: 747–756. doi: 10.3758/s13415-013-0191-5 PMID: 23943512

64. Fleming SM, Whiteley L, Hulme OJ, Sahani M, Dolan RJ. Effects of Category-Specific Costs on Neural Systems for Perceptual Decision-Making. Journal of Neurophysiology 2010; 103: 3238–3247. doi: 10.1152/jn.01084.2009 PMID: 20357071

65. Fleming SM, Thomas CL, Dolan RJ. Overcoming status quo bias in the human brain. Proceedings of the National Academy of Sciences 2010; 107: 6005–6009. doi: 10.1073/pnas.0910380107 PMID: 20231462

66. Guitart-Masip M, Fuentemilla L, Bach DR, Huys QJM, Dayan P, Dolan RJ, et al. Action Dominates Valence in Anticipatory Representations in the Human Striatum and Dopaminergic Midbrain. Journal of Neuroscience 2011; 31: 7867–7875. doi: 10.1523/JNEUROSCI.6376-10.2011 PMID: 21613500

67. Guitart-Masip M, Chowdhury R, Sharot T, Dayan P, Düzel E, Dolan RJ. Action controls dopaminergic enhancement of reward representations. Proc Natl Acad Sci USA 2012; 109: 7511–7516. doi: 10.1073/pnas.1202229109/-/DCSupplemental/pnas.201202229SI.pdf PMID: 22529363

68. Herz DM, Christensen MS, Bruggemann N, Hulme OJ, Ridderinkhof KR, Madsen KH, et al. Motivational Tuning of Fronto-Subthalamic Connectivity Facilitates Control of Action Impulses. Journal of Neuroscience 2014; 34: 3210–3217. doi: 10.1523/JNEUROSCI.4081-13.2014 PMID: 24573279

69. Hu S, Tseng Y-C, Winkler AD, Li C-SR. Neural bases of individual variation in decision time. Hum Brain Mapp 2013. doi: 10.1002/hbm.22347.

70. Jahfari S, Waldorp L, van den Wildenberg WPM, Scholte HS, Ridderinkhof KR, Forstmann BU. Effective Connectivity Reveals Important Roles for Both the Hyperdirect (Fronto-Subthalamic) and the Indirect (Fronto-Striatal-Pallidal) Fronto-Basal Ganglia Pathways during Response Inhibition. Journal of Neuroscience 2011; 31: 6891–6899. doi: 10.1523/JNEUROSCI.5253-10.2011 PMID: 21543619

71. Kirsch P, Schienle A, Stark R, Sammer G, Blecker C, Walter B, et al. Anticipation of reward in a nonaversive differential conditioning paradigm and the brain reward system:. NeuroImage 2003; 20: 1086–1095. doi: 10.1016/S1053-8119(03)00381-1 PMID: 14568478

72. Krebs RM, Schott BH, Duzel E. Personality Traits Are Differentially Associated withPatterns of Reward and Novelty Processing in theHuman Substantia Nigra/Ventral Tegmental Area. Biol Psychiatry 2009; 65: 103–110. doi: 10.1016/j.biopsych.2008.08.019 PMID: 18835480

73. Krebs RM, Heipertz D, Schuetze H, Duzel E. Novelty increases the mesolimbic functional connectivity of the substantia nigra/ventral tegmental area (SN/VTA) during reward anticipation: Evidence from high-resolution fMRI. NeuroImage 2011; 58: 647–655. doi: 10.1016/j.neuroimage.2011.06.038 PMID: 21723396

74. Krebs RM, Boehler CN, Roberts KC, Song AW, Woldorff MG. The Involvement of the Dopaminergic Midbrain and Cortico-Striatal-Thalamic Circuits in the Integration of Reward Prospect and Attentional Task Demands. Cerebral Cortex 2012; 22: 607–615. doi: 10.1093/cercor/bhr134 PMID: 21680848

75. Lehéricy S. Motor control in basal ganglia circuits using fMRI and brain atlas approaches. Cerebral Cortex 2005; 16: 149–161. doi: 10.1093/cercor/bhi089 PMID: 15858164

76. Lévesque J, Beauregard M, Mensour B. Effect of neurofeedback training on the neural substrates of selective attention in children with attention-deficit/hyperactivity disorder: A functional magnetic resonance imaging study. Neurosci Lett 2006; 394: 216–221. doi: 10.1016/j.neulet.2005.10.100 PMID: 16343769

77. Leunissen I, Coxon JP, Geurts M, Caeyenberghs K, Michiels K, Sunaert S, et al. Disturbed cortico-subcortical interactions during motor task switching in traumatic brain injury. Hum Brain Mapp 2012; 34: 1254–1271. doi: 10.1002/hbm.21508 PMID: 22287257

78. Marchand WR, Lee JN, Suchy Y, Garn C, Chelune G, Johnson S, et al. Functional architecture of the cortico-basal ganglia circuitry during motor task execution: Correlations of strength of functional connectivity with neuropsychological task performance among female subjects. Hum Brain Mapp 2012; 34: 1194–1207. doi: 10.1002/hbm.21505 PMID: 22287185

79. Menz MM, Buchel C, Peters J. Sleep Deprivation Is Associated with Attenuated Parametric Valuation and Control Signals in the Midbrain during Value-Based Decision Making. Journal of Neuroscience 2012; 32: 6937–6946. doi: 10.1523/JNEUROSCI.3553-11.2012 PMID: 22593062

80. Monchi O, Petrides M, Strafella AP, Worsley KJ, Doyon J. Functional role of the basal ganglia in the planning and execution of actions. Ann Neurol 2006; 59: 257–264. doi: 10.1002/ana.20742 PMID: 16437582

81. Murray GK, Corlett PR, Clark L, Pessiglione M, Blackwell AD, Honey G, et al. Substantia nigra/ventral tegmental reward prediction error disruption in psychosis. Mol Psychiatry 2007; 13: 267–276. doi: 10.1038/sj.mp.4002058.

82. Preuschoff K, Bossaerts P, Quartz SR. Neural Differentiation of Expected Reward and Risk in Human Subcortical Structures. Neuron 2006; 51: 381–390. doi: 10.1016/j.neuron.2006.06.024 PMID: 16880132

83. Prodoehl J, Yu H, Wasson P, Corcos DM, Vaillancourt DE. Effects of Visual and Auditory Feedback on Sensorimotor Circuits in the Basal Ganglia. Journal of Neurophysiology 2008; 99: 3042–3051. doi: 10.1152/jn.01108.2007 PMID: 18287549

84. Ray Li C-S, Yan P, Sinha R, Lee T-W. Subcortical processes of motor response inhibition during a stop signal task. NeuroImage 2008; 41: 1352–1363. doi: 10.1016/j.neuroimage.2008.04.023 PMID: 18485743

85. Robinson S, Basso G, Soldati N, Sailer U, Jovicich J, Bruzzone L, et al. A resting state network in the motor control circuit of the basal ganglia. BMC Neuroscience 2009; 10: 137. doi: 10.1186/1471-2202-10-137 PMID: 19930640

86. Schott BH. Activation of Midbrain Structures by Associative Novelty and the Formation of Explicit Memory in Humans. Learning & Memory 2004; 11: 383–387. doi: 10.1101/lm.75004.

87. Schott BH, Minuzzi L, Krebs RM, Elmenhorst D, Lang M, Winz OH, et al. Mesolimbic Functional Magnetic Resonance Imaging Activations during Reward Anticipation Correlate with Reward-Related Ventral Striatal Dopamine Release. Journal of Neuroscience 2008; 28: 14311–14319. doi: 10.1523/JNEUROSCI.2058-08.2008 PMID: 19109512

88. Shohamy D, Myers CE, Kalanithi J, Gluck MA. Basal ganglia and dopamine contributions to probabilistic category learning. Neuroscience and Biobehavioral Reviews 2008; 32: 219–236. doi: 10.1016/j.neubiorev.2007.07.008 PMID: 18061261

89. Vaillancourt DE, Yu H, Mayka MA, Corcos DM. Role of the basal ganglia and frontal cortex in selecting and producing internally guided force pulses. NeuroImage 2007; 36: 793–803. doi: 10.1016/j.neuroimage.2007.03.002 PMID: 17451971

90. Wittmann BC, Schott BH, Guderian S, Frey JU, Heinze H-J, Duzel E. Reward-Related fMRI Activation of Dopaminergic Midbrain Is Associated with Enhanced Hippocampus- Dependent Long-Term Memory Formation. Neuron 2005; 45: 459–467. doi: 10.1016/j.neuron.2005.01.010 PMID: 15694331

91. Wittmann BC, Bunzeck N, Dolan RJ, Düzel E. Anticipation of novelty recruits reward system and hippocampus while promoting recollection. NeuroImage 2007; 38: 194–202. doi: 10.1016/j.neuroimage.2007.06.038 PMID: 17764976